# Groundwater-native Fe(II) oxidation prior to aeration with $H_2O_2$ to enhance As(III) removal

Roy, Mrinal; van Genuchten, Case M.; Rietveld, Luuk; van Halem, Doris

**DOI**
10.1016/j.watres.2022.119007

**Publication date**
2022

**Document Version**
Final published version

**Published in**
Water Research

Water Research 223 (2022) 119007

Contents lists available at ScienceDirect

Water Research

journal homepage: www.elsevier.com/locate/watres

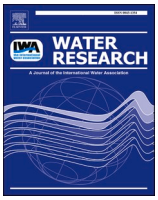

# Groundwater-native Fe(II) oxidation prior to aeration with $H_2O_2$ to enhance As(III) removal

Mrinal Roy [a,*], Case M. van Genuchten [b], Luuk Rietveld [a], Doris van Halem [a]

[a] Water Management Department, Faculty of Civil Engineering and Geosciences, Delft University of Technology, Stevinweg 1, Delft CN 2628, the Netherlands
[b] Department of Geochemistry, Geological Survey of Denmark and Greenland, Copenhagen DK 1350, Denmark

ARTICLE INFO

*Keywords:*
Arsenic
Iron
Hydrogen peroxide
Groundwater
Drinking water

ABSTRACT

Groundwater contaminated with arsenic (As) must be treated prior to drinking, as human exposure to As at toxic levels can cause various diseases including cancer. Conventional aeration-filtration applied to anaerobic arsenite (As(III)) contaminated groundwater can remove As(III) by co-oxidizing native iron (Fe(II)) and As(III) with oxygen ($O_2$). However, the As(III) removal efficiency of conventional aeration can be low, in part, because of incomplete As(III) oxidation to readily-sorbed arsenate (As(V)). In this work, we investigated a new approach to enhance As(III) co-removal with native Fe(II) by the anaerobic addition of hydrogen peroxide ($H_2O_2$) prior to aeration. Experiments were performed to co-oxidize Fe(II) and As(III) with $H_2O_2$ (anaerobically), $O_2$ (aerobically), and by sequentially adding of $H_2O_2$ and $O_2$. Aqueous As(III) and As(V) measurements after the reaction were coupled with solid-phase speciation by Fe and As K-edge X-ray absorption spectroscopy (XAS). We found that complete anaerobic oxidation of 100 μM Fe(II) with 100 μM $H_2O_2$ resulted in co-removal of 95% of 7 μM As (III) compared to 44% with 8.0-9.0 mg/L dissolved $O_2$. Furthermore, we found that with 100 μM Fe(II), the initial Fe(II):$H_2O_2$ ratio was a critical parameter to remove 7 μM As(III) to below the 10 μg/L (0.13 μM) WHO guideline, where ratios of 1:4 (mol:mol) Fe(II):$H_2O_2$ led to As(III) removal matching that of 7 μM As(V). The improved As (III) removal with $H_2O_2$ was found to occur partly because of the well-established enhanced efficiency of As(III) oxidation in Fe(II)+$H_2O_2$ systems relatively to Fe(II)+$O_2$ systems. However, the XAS results unambiguously demonstrated that a large factor in the improved As(III) removal was also due to a systematic decrease in crystallinity, and thus increase in specific surface area, of the generated Fe(III) (oxyhydr)oxides from lepidocrocite in the Fe(II)+$O_2$ system to poorly-ordered Fe(III) precipitates in the Fe(II)+$H_2O_2$ system. The combined roles of $H_2O_2$ (enhanced As(III) oxidation and structural modification) can be easily overlooked when only aqueous species are measured, but this dual impact must be considered for accurate predictions of As removal in groundwater treatment.

## 1. Introduction

An estimated 94-220 million people are exposed to naturally occurring arsenic (As) in groundwater (mainly as arsenite (As(III))) at levels above the World Health Organization (WHO) drinking water guideline of 10 μg/L (0.13 μM) (Podgorski and Berg, 2020). Exposure to As-contaminated water can pose major threats to human health causing diseases such as skin, bladder and lung cancers, reproductive disorders, and neuro-developmental problems in children (Kapaj et al., 2006; Tseng, 1977). Therefore, it is crucial that groundwater contaminated with toxic levels of As be treated prior to drinking.

Conventional aeration-filtration is a common treatment method that involves aerating anaerobic As(III)-rich groundwater that contains co-occurring iron (Fe(II)), followed by filtration of the generated solids (Gude et al., 2016; Hug and Leupin, 2003; Roberts et al., 2004). This method relies on As(III) and Fe(II) co-oxidation by $O_2$ to form particulate Fe(III) (oxyhydr)oxides (or Fe solids) that can bind As (Bora et al., 2016; Gude et al., 2016). Compared to other techniques, aeration-filtration is advantageous as it is economically attractive, no dosing of chemicals is required, it removes various groundwater contaminants (Fe(II), ammonium, manganese) simultaneously, and it generates biologically stable drinking water (low in nutrients), thereby ensuring microbial safety in distribution networks (Annaduzzaman et al., 2021a; Gude et al., 2017). While conventional aeration-filtration is applied widely in

* Corresponding author.
*E-mail address:* m.roy-1@tudelft.nl (M. Roy).

https://doi.org/10.1016/j.watres.2022.119007
Received 16 June 2022; Received in revised form 17 August 2022; Accepted 18 August 2022
Available online 19 August 2022

groundwater treatment and Fe solids are very good adsorbents for As, this conventional approach can be ineffective for As(III) removal, which often demands additional dosing of Fe to meet drinking water guidelines (Annaduzzaman et al., 2018; Annaduzzaman et al., 2021b; Sharma et al., 2016). For example, previous studies have shown that co-removal of As(III) with Fe(II) through aeration-filtration only yields between 8-50% removal, depending on the initial As concentration, As:Fe ratio, and the presence of other competing ions (i.e. manganese, phosphate) (van Genuchten and Ahmad, 2020; Holm and Wilson, 2006; Li et al., 2016).

The low efficacy of As(III) co-removal with native Fe(II) during aeration-filtration can be due to several factors. First, Fe solids generated by aeration (by $O_2$) can be moderately crystalline (Ahmad et al., 2019) with a lower reactive specific surface area than the poorly-ordered Fe solids generated with stronger oxidants, such as HOCl and $KMnO_4$ (Ahmad et al., 2019). Second, Fe solids have orders of magnitude lower sorption affinity for As(III) than oxidized arsenate (As(V)) and As(III) oxidation during aeration is slow and partial (Bissen and Frimmel, 2003; Gude et al., 2017; Roberts et al., 2004). Third, the relatively high pH resulting from $CO_{2(g)}$ degassing during groundwater aeration creates a less favourable environment for As(V) adsorption (Annaduzzaman et al., 2021b; Dixit and Hering, 2003), which can be minimized by avoiding aeration. Thus, the co-removal of groundwater As(III) with native Fe(II) can be optimized by forming poorly-ordered solids, with high reactive surface area, and by co-oxidizing As(III) effectively and rapidly prior to aeration to minimize pH increase induced by $CO_{2(g)}$ efflux.

The addition of hydrogen peroxide ($H_2O_2$) is an attractive option for anaerobic As(III) and Fe(II) co-oxidation because $H_2O_2$ reacts rapidly with Fe(II), and is relatively inexpensive to generate on- or off-site, and is considered a green alternative to harsher chemical oxidants because of its non-toxic reaction products (Bandaru et al., 2020; Pham et al., 2012a, 2012b). Additionally, $H_2O_2$ is an intermediate formed during Fe(II) oxidation by $O_2$ (Hug and Leupin, 2003) and may as such be considered a natural additive in anaerobic groundwater treatment. In principle, the presence of $H_2O_2$ in As(III) and Fe(II)-rich solutions is beneficial because it oxidizes Fe(II) at a rate four orders of magnitude higher than $O_2$ (Bandaru et al., 2020; King and Farlow, 2000; King, 1998), which can result in the generation of poorly-ordered Fe(III) solids (Bandaru et al., 2020; van Genuchten and Peña, 2017). In addition, while direct As(III) oxidation by $H_2O_2$ is kinetically limited, the oxidation of Fe(II) by $H_2O_2$ leads to a high stoichiometric yield of reactive oxygen species (ROS), such as *OH or Fe(IV), that can effectively oxidize As(III) (Hug and Leupin, 2003). The theoretical ROS yield per mol of oxidized Fe(II) is 1:1 for $H_2O_2$ compared to 1:3 for $O_2$ (Hug and Leupin, 2003), which would translate to more As(III) co-oxidation per mole of oxidized Fe(II) if $H_2O_2$ is applied. While Fenton-type systems (i.e. those containing Fe(II)+$H_2O_2$) have been investigated in the context of As(III) removal previously (Bandaru et al., 2020; Catrouillet et al., 2020), most studies performed, are over-dosing $H_2O_2$ in solutions open to the atmosphere, initially containing $O_2$. Careful control of the $H_2O_2$ input and thus the Fe(II):$H_2O_2$ ratio, could thus be more effective, particularly in the case of treating anaerobic groundwater, because it can optimize the use of natural Fe(II), minimize the consumption of $H_2O_2$, and can avoid an increase in pH due to $CO_{2(g)}$ efflux.

In this study a novel approach is therefore proposed to enhance As(III) removal in groundwater with the native Fe(II), through anaerobic oxidation of the native Fe(II) by $H_2O_2$ prior to aeration. Moreover, we compared the impact of oxidizing Fe(II) with $O_2$ (aerobically), $H_2O_2$ (anaerobically), and sequentially with $H_2O_2$ (anaerobically) followed by $O_2$ (aerobically) on As(III) removal. The reactions were tracked by aqueous As(III) and As(V) speciation measurements and by characterization of the solid reaction products by synchrotron-based Fe and As K-edge X-ray absorption spectroscopy (XAS). In addition, we examined the impact of under- and over-dosage of $H_2O_2$ (anaerobically) on the extent of Fe(II) and As(III) co-oxidation. Finally, we validated this approach by studying $H_2O_2$ addition to Fe(II)-containing raw anaerobic groundwater

## 2. Materials and methods

### 2.1. Chemicals

Ultrapure water (18.2 mΩ.cm) was used to prepare all experimental solutions and was spiked with to 2.5 mM $NaHCO_3$ and 10 mM NaCl by dissolving 0.32 g of sodium bicarbonate (J.T. Baker™) and 0.88 g of sodium chloride (J.T. Baker™) in 1.5 L. The concentration of $NaHCO_3$ (2.5 mM) and NaCl (10 mM) were selected to achieve an alkalinity and conductivity (990 μS/cm) similar to previous studies in synthetic groundwater (Ahmad et al., 2019; van Genuchten et al., 2012). As(III), As(V), and Fe(II) were added from stock solutions, which were freshly prepared daily. Stock solutions were generated by dissolving defined amounts of sodium (meta)arsenite ($NaAsO_2$) or sodium arsenate dibasic heptahydrate ($Na_2HAsO_4.7H_2O$) (Sigma-Aldrich) to ultrapure water and ferrous sulfate heptahydrate ($FeSO_4.7H_2O$) (Sigma-Aldrich)) to 1 mM HCl respectively. $H_2O_2$ stock solutions were also freshly diluted with defined volumes of the 30% w/w $H_2O_2$ solution (Sigma-Aldrich) in ultrapure water. For pH adjustment, 1 M HCl or 1 M NaOH (Merck Millipore) was used.

### 2.2. Experimental setup and procedure

The experiments were conducted at room temperature (20±3 °C) in 2 L glass jars with perforated lids (Fig. S1). The jars initially contained 1 L of ultrapure water (18.2 mΩ.cm) with 2.5 mM $NaHCO_3$, 10 mM NaCl, and 7 μM As(III) or As(V). The solution was then purged with $N_{2(g)}$ to obtain dissolved $O_2$ concentrations of <0.1 mg/L and the pH was set to 7.3-7.5. Next, Fe(II) was added to the $O_2$-purged solution. The oxidation of Fe(II) was initiated by dosing $H_2O_2$ or $O_2$ alone or by sequentially dosing $H_2O_2$ followed by $O_2$ ($H_2O_2$+$O_2$). To dose $O_2$, an air-pump was used to raise the dissolved $O_2$ to 8.0-9.0 mg/L (from initial levels of <0.1 mg/L) after adding Fe(II). The solution was mixed with a magnetic stirrer (LABINCO L23) at 150 rpm for 30 min after Fe(II) oxidation began. In $H_2O_2$ experiments, $N_{2(g)}$ was continuously purged throughout the mixing period to minimize the impact of atmospheric $O_2$ influx and to maintain dissolved $O_2$ levels <0.1 mg/L. For the sequential $H_2O_2$+$O_2$ experiments, partial Fe(II) oxidation was performed first by adding $H_2O_2$ and mixing for 5 min under continuous $N_{2(g)}$ purging (dissolved $O_2$ <0.1 mg/L), followed by $O_2$ dosing using the air-pump (dissolved $O_2$ = 8.0-9.0 mg/L) for the remaining 25 min. The pH of all solutions was maintained between 7.3-7.5 during experiments by manual additions of 1 M NaOH or 1 M HCl. The pH and dissolved $O_2$ were monitored using a multimeter (WTW™ MultiLineTM Multi 3630 IDS).

### 2.3. Experimental conditions

To determine the impact of various Fe(II) oxidant conditions on As(III) co-removal, experiments were performed in the $H_2O_2$, $O_2$, and sequential $H_2O_2$+$O_2$ systems by completely oxidizing 100 μM Fe(II) with 100 μM $H_2O_2$ (anaerobically), 8.0-9.0 mg/L $O_2$ (aerobically), or sequentially by 5, 10, 20, or 40 μM $H_2O_2$ (anaerobically) followed by $O_2$ (aerobically). Another set of experiments was performed to examine the effect of $H_2O_2$ concentration (and thus Fe(II):$H_2O_2$ ratio) on the co-oxidation and removal of 100 μM Fe(II) and 7 μM As(III). For these experiments, the $H_2O_2$ concentrations (i.e. 10, 20, 40, 60, 100, 200, 300, and 400 μM) were selected to span the stoichiometric amount required for total Fe(II) oxidation. A set of experiments was also repeated with initial 7 μM As(V) in place of As(III). In addition to laboratory tests, experiments were performed using raw Dutch groundwater, which was obtained directly from the influent of a drinking water treatment plant. For these experiments, the raw anaerobic water (initial composition given in Table S1) was spiked with 7 μM As(III). The removal of As(III) was investigated by completely oxidizing the groundwater-native Fe(II) with either $H_2O_2$ or $O_2$. In the $H_2O_2$ experiments with raw groundwater, $N_{2(g)}$ was not used to decrease the dissolved $O_2$ to <0.1 mg/L. All

experiments were replicated at least twice. A schematic overview of the experimental conditions is shown in Fig. S1.

### 2.4. Chemical analysis

During the 30 min reaction time, filtered and unfiltered water samples were collected at 0, 2, 5, 10, 20, and 30 min. Filtration was performed with 0.2 μm polyethersulfone filters (Macherey-Nagel GmbH & Co. KG). Immediately after collection, the samples were acidified with 1% (v/v) ultrapure nitric acid (ROTIPURAN® Ultra 69%) to stop further reactions and dissolve any solids. Acidified samples were stored at 4 °C until analysis. We refer to Fe measured in the filtered solution as Fe(II), which we verified by measuring Fe(II) in a subset of filtered samples using an Fe cell test kit (Merck Millipore). For dissolved As speciation, we followed the approach described in Gude et al. (2018), which is based on using an anionic exchange resin (Amberlite* IRA-402 chlorite) to separate non-ionic As(III) and negatively-charged As(V). The unfiltered samples were used to determine the total Fe and Fe(III) concentration, where the difference between total Fe and dissolved Fe represented the Fe(III). The samples were analyzed for As and Fe (in triplicates) by inductively coupled plasma mass spectrometry (ICP-MS, Analytikal Jena model PlasmaQuant MS).

### 2.5. X-ray absorption spectroscopy

#### 2.5.1. Data collection

Solids for XAS analysis were collected using filter papers at the end of the oxidation experiments. The filter papers with solids attached were stored at -80 °C before affixing the sample (filter and solids) to custom sample holders using Kapton tape. Fe and As K-edge XAS data were collected at beam line 2–2 of the Stanford Synchrotron Radiation Lightsource (SSRL, Menlo Park, USA). Fe K-edge XAS data were recorded at room temperature out to $k = 13$ Å$^{-1}$ and As K-edge XAS data were recorded at liquid nitrogen temperatures (≈80 °K) in fluorescence mode out to $k = 14$ Å$^{-1}$. For beam calibration, the maximum of the first derivative of Fe(0) and Au(0) foils was set to 7112 eV and 11919 eV for Fe and As data, respectively. Spectral alignment, averaging and background subtraction of individual spectra were performed using SixPack software (Webb, 2005), following standard procedures described in van Genuchten et al. (2012). Extraction of the Fe K-edge EXAFS spectra was performed using $k^3$-weighting and the Fe K-edge EXAFS spectra were Fourier-transformed over the $k$-range 2 to 11 Å$^{-1}$ using a Kaiser-Bessel window with dk of 3 Å$^{-1}$.

#### 2.5.2. Data analysis

The Fe K-edge EXAFS spectra were analysed by liner combination fits (LCFs) ($k$ = 2-11 Å$^{-1}$) with the SixPack software (Webb, 2005) using the EXAFS spectra of three reference Fe(III) (oxyhydr)oxides: moderately crystalline lepidocrocite (Lp), nanocrystalline 2-line ferrihydrite (2LFh), and highly disordered oxyanion-rich hydrous ferric oxide (oxy-HFO). These three reference Fe(III) (oxyhydr)oxides were selected based on previous studies that report these references reproduced the Fe(III) solids generated by Fe(II) oxidation using a range of chemical oxidants (Ahmad et al., 2019; van Genuchten et al., 2018; van Genuchten et al., 2014). The fraction of the three references in each experimental sample derived from the LCFs was normalized to one.

The As K-edge XANES spectra were analyzed by LCFs using SixPack software to determine the fraction of adsorbed As(III) and As(V). The LCFs were performed with a fit range of 11860 to 11880 eV using reference spectra of As(III) and As(V) adsorbed to 2-line ferrihydrite. In the LCFs, negative fractions of the reference spectra were not allowed and the component sum was not constrained to 1. The concentration of adsorbed As(III) and As(V) was calculated by multiplying the LCF-derived fraction of As(III) and As(V) by the concentration of total As removed from solution determined by ICP-MS. We use the As K-edge XAS data primarily to determine the oxidation state of As bound to the solid phase. Shell-by-shell fits of the EXAFS spectra were not performed partly because many of our samples contained multiple As oxidation states, which complicates the interpretation of shell fits (van Genuchten et al., 2012; van Genuchten and Ahmad, 2020). Further details on XAS sample preparation and data collection are given in the Supplementary Materials.

## 3. Results and discussion

### 3.1. Solid-phase Fe structure and its relation to Fe(II) oxidation kinetics

Fig. 1(A) and (B) shows the Fe K-edge EXAFS spectra, and corresponding Fourier transforms, of the three reference Fe(III) (oxyhydr) oxides and the experimental samples generated in the $O_2$, $H_2O_2$, and sequential $H_2O_2$+$O_2$ systems. Comparing the EXAFS spectral features of Lp, 2LFh, and oxy-HFO, a peak can be observed in Lp near 7.84 Å$^{-1}$, which dampened in 2LFh and disappeared in oxy-HFO. In addition, the first oscillation from 4-5 Å$^{-1}$ is asymmetric in Lp but becomes more symmetric for 2LFh and oxy-HFO, with the oscillations at $k > 8$ Å$^{-1}$ becoming more broad with lower amplitude from Lp to 2LFh to oxy-HFO. These features are consistent with a progressive decrease in structural order from Lp to 2LFh to oxy-HFO (Toner et al., 2009; van Genuchten et al., 2012). Visual comparison of the EXAFS spectra of the experimental solids indicates that the EXAFS spectrum of the sample generated by $O_2$ oxidation closely matched the line shape and phase of the Lp EXAFS spectrum. However, a gradual and systematic shift in EXAFS features from Lp to 2LFh and oxy-HFO was observed with an increasing concentration of initial $H_2O_2$, and thus increasing fraction of Fe(II) oxidized by $H_2O_2$. As shown in the Fourier-transform (Fig. 1(B)), these changes in the EXAFS spectra of the samples correspond to a systematic decrease in the amplitude of second-shell peak, which arises from Fe-Fe atomic pairs, suggesting a progressive decrease in structural order with increasing $H_2O_2$ concentration (Toner et al., 2009; van Genuchten et al., 2012). We assign the second-shell peak with Fe-Fe atomic pairs because no other atoms can be present in the second shell of Fe at high enough concentrations to contribute significantly to this peak (i.e., As can occur in the second shell, but its concentration in the solid phase is too low to be detected in the Fe data).

The LCFs of the EXAFS spectra (Fig. 1(C); Table S2) confirmed the decrease in Fe(III) precipitate crystallinity with increasing initial $H_2O_2$ concentration. The LCFs indicated that the highest fraction of moderately crystalline Lp was present in the sample generated by $O_2$ oxidation of Fe(II). The fraction of Lp in the solids derived by LCFs decreased systematically in favor of poorly-ordered Fe(III) precipitates (2LFh and oxy-HFO) with increasing Fe(II) oxidation by $H_2O_2$. Lp was not detected in the experiments where 100% of Fe(II) was oxidized by $H_2O_2$. Instead, the solids generated by Fe(II) oxidation with $H_2O_2$ consisted of 100% poorly-ordered Fe(III) precipitates (Fig. 1(C); Table S2). Such formation of a higher fraction of poorly-ordered Fe solids with $H_2O_2$ compared to $O_2$ is consistent with the previously reported impact of Fe(II) oxidation rate on Fe(III) precipitate structure (Ahmad et al., 2019; Bandaru et al., 2020; Catrouillet et al., 2020; van Genuchten and Peña, 2017). The low oxidation rate of Fe(II) with $O_2$ allows the presence of aqueous Fe(II) to catalyze the crystallization of freshly-precipitated Fe(III) precursors into Lp (Ahmad et al., 2019; Pedersen et al., 2005). By contrast, $H_2O_2$ oxidizes aqueous Fe(II) too rapidly to permit any Fe(II)-catalyzed crystallization of newly-formed Fe(III) precipitates (Ahmad et al., 2019; Pedersen et al., 2005).

To verify rapid Fe(II) oxidation with $H_2O_2$, the kinetics of Fe(III) generation was tested over 30 min for the same oxidation conditions (Fig. 1(D)) as used to generate the solids for XAS analysis (i.e. oxidation of 100μM Fe(II) in the $O_2$, $H_2O_2$, and $H_2O_2$+$O_2$ systems). It was observed that all the Fe(II) was oxidized within 10 min regardless of the oxidant (Fig. 1(D)). However, with 100 μM $H_2O_2$, complete Fe(II) oxidation was faster (<2 min) than with $O_2$ (between 5-10 min), which is in-line with previous research (Bandaru et al., 2020; King and Farlow, 2000; King,

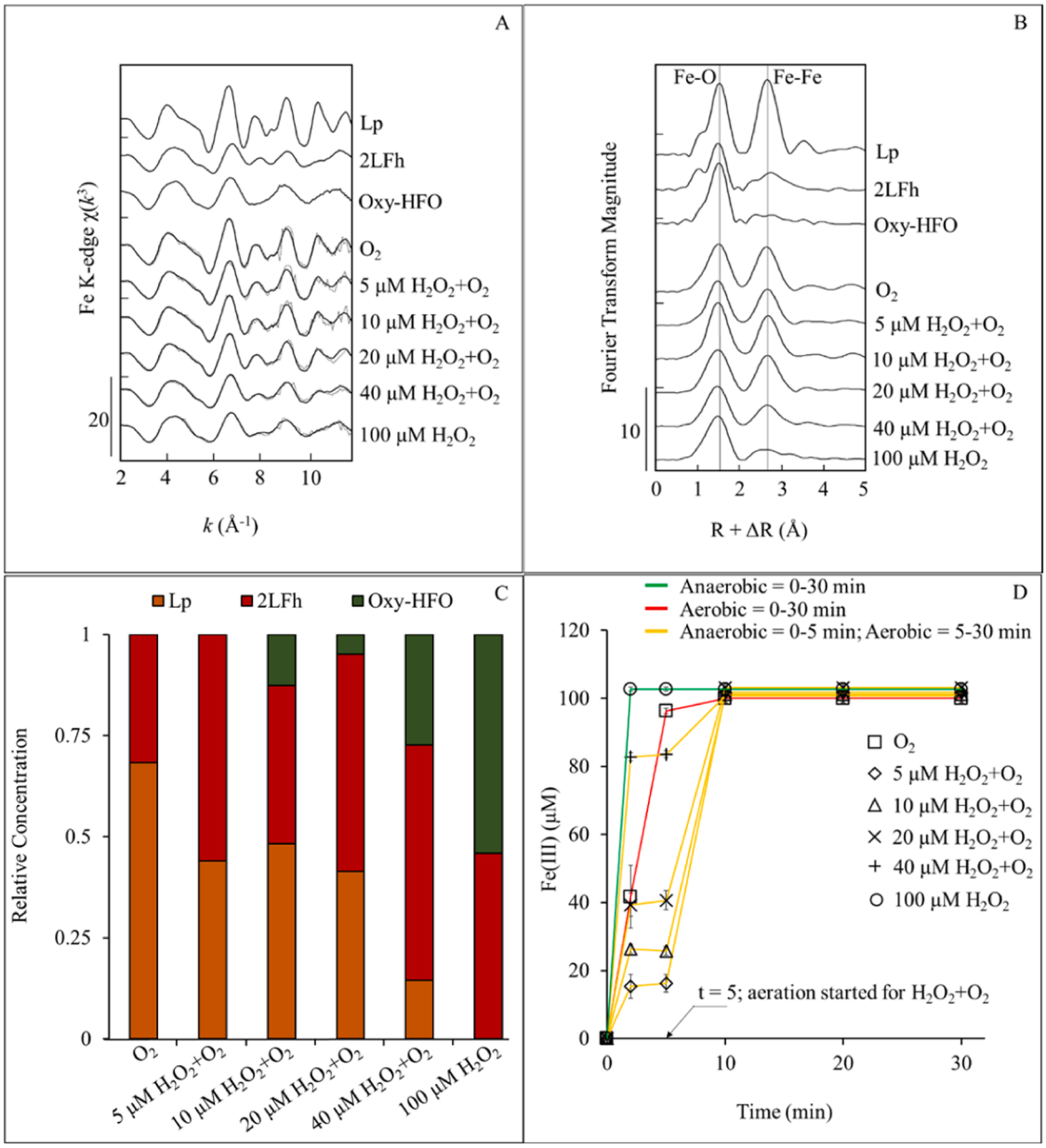


**Fig. 1.** Fe K-edge EXAFS spectra and corresponding Fourier transforms of the Fe solids (A and B), relative concentration of lepidocrocite (Lp), 2-line ferrihydrite (2LFh), and oxyanion-rich hydrous ferric oxide (oxy-HFO) in the Fe solids determined from LCFs (C), and kinetics of Fe(III) generation over 30 min when 100±3 μM Fe(II) was oxidized by 8.0-9.0 mg/L $O_2$ (aerobically; t = 0-30 min), 100 μM $H_2O_2$ (anaerobically; t = 0-30 min), or sequentially by 5, 10, 20, or 40 μM $H_2O_2$ (anaerobically; t = 0-5 min) followed by 8.0-9.0 mg/L $O_2$ (aerobically; t = 5-30 min). The LCF output is overlain on the experimental data in panel A. Solutions initially contained 7±0.5 μM As(III), 2.5 mM $NaHCO_3$, and 10 mM NaCl. All Fe(III) formed solids and no dissolved Fe(III) was detected (data not shown). Data points and error bars represent the average and standard deviation of the samples obtained from replicate experiments.

1998). In the sequential experiments with initial 5, 10, 20 or 40 μM $H_2O_2$, Fe(II) oxidation was fast but incomplete, with the expected stoichiometric 2:1 mol:mol ratio of Fe(II) oxidation by $H_2O_2$ observed for all $H_2O_2$ experiments. This 2:1 stoichiometry led to residual Fe(II) concentrations of 85, 76, 64, and 17 μM at 5 min using $H_2O_2$ dosages of 5, 10, 20, and 40 μM, respectively, with the remaining Fe(II) oxidized by $O_2$ added by aeration at t > 5 min. These results show that anaerobic Fe (II) oxidation with $H_2O_2$ closely followed the expected 2:1 ratio and favoured the formation of poorly-ordered Fe(III) solids, in contrast to $O_2$, due to its more rapid oxidation rate with Fe(II).

### 3.2. As(III) removal by Fe solids

Fig. 2(A) shows the co-removal of initial 7±0.5 μM As(III) when oxidizing 100±3 μM Fe(II) in the $O_2$, $H_2O_2$, and sequential $H_2O_2$+$O_2$ systems. Comparing the different oxidant conditions, As(III) removal was the lowest in the $O_2$ system, where the residual dissolved As concentration (t = 30 min) was 3.8±0.2 μM (44% removal). In the sequential $H_2O_2$+$O_2$ system, As(III) removal was moderate and the residual dissolved As concentration (t = 30 min) decreased systematically (3.6±0.2, 2.9±0.4, 2.6±0.1, and 1.3±0.10 μM) with increasing initial $H_2O_2$ concentration (5, 10, 20, and 40 μM $H_2O_2$). The most removal of initial As(III) was observed using 100 μM $H_2O_2$, with a residual dissolved As concentration (t = 30 min) of 0.4±0.1 μM (95% removal). Thus, the poorest As removal was observed when Fe(II) was oxidized by $O_2$ alone and removal increased with an increase in the fraction of Fe(II) oxidized by $H_2O_2$. This trend is consistent with the increasing fraction of poorly-ordered Fe solids with increasing initial $H_2O_2$ concentration (Fig. 1(C)),

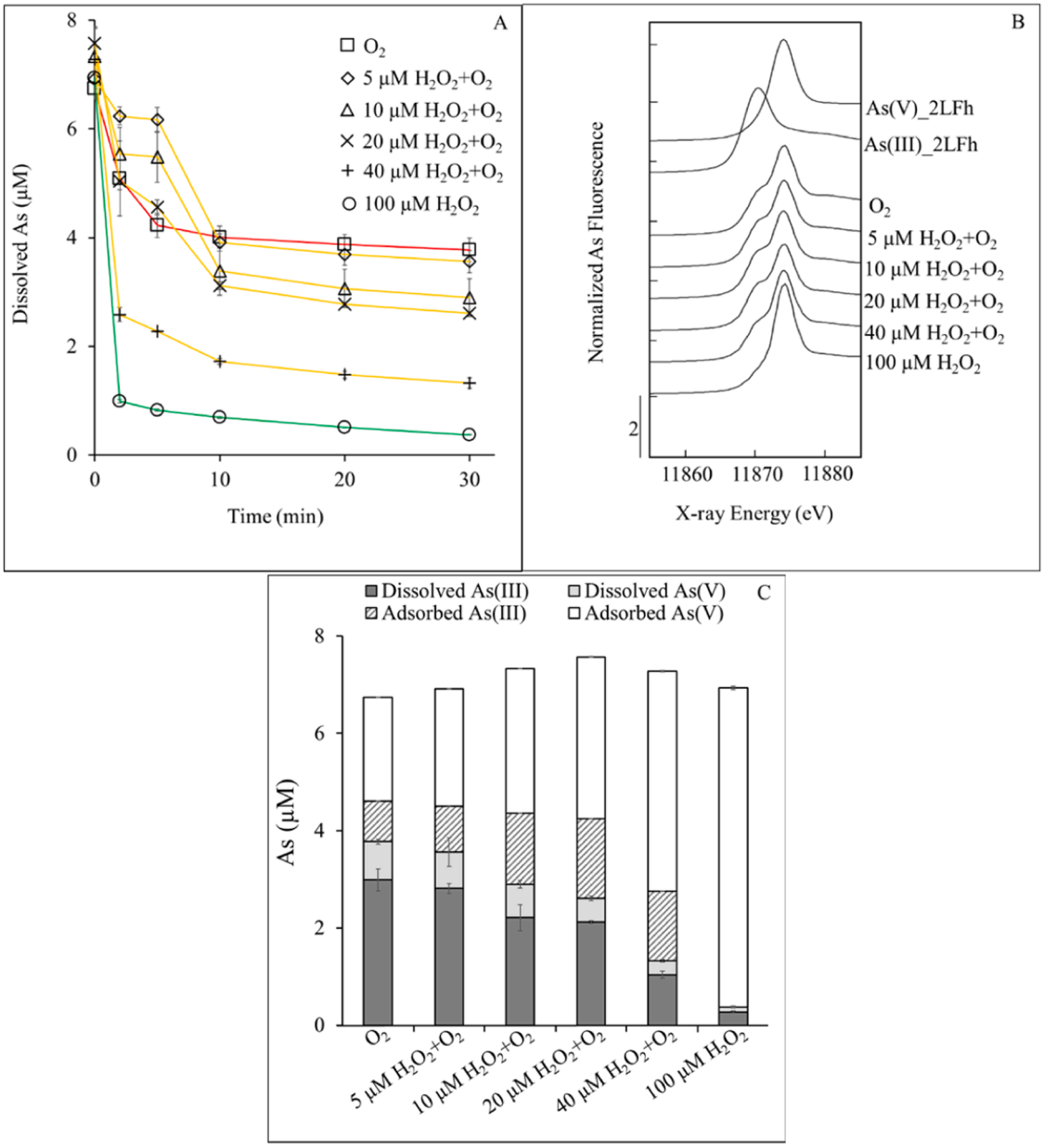


**Fig. 2.** Removal of initial As(III) over 30 min (A), As K-edge XANES spectra of the generated Fe solids (B), and As speciation at the experiment end (t = 30 min) when 100±3 μM Fe(II) was oxidized by 8.0-9.0 mg/L $O_2$ (aerobically; t = 0-30 min) (red line), 100 μM $H_2O_2$ (anaerobically; t = 0-30 min) (green line), or sequentially by 5, 10, 20, or 40 μM $H_2O_2$ (anaerobically; t = 0-5 min) followed by 8.0-9.0 mg/L $O_2$ (aerobically; t = 5-30 min) (yellow line). Solutions initially contained 7±0.5 μM As (III), 2.5 mM $NaHCO_3$, and 10 mM NaCl. Data points and error bars represent the average and standard deviation of the samples obtained from replicate experiments.

as observed in the previous section.

Fig. 2(B) shows the As K-edge XANES spectra of samples generated in the $O_2$, $H_2O_2$, and sequential $H_2O_2$+$O_2$ systems, with the LCFs of the XANES spectra reported in Table S3. The XANES spectra show that As(V) was the dominant species adsorbed on the solids, based on the position of the absorption maximum near 11875 eV. The predominance of solid-phase As(V) was confirmed by the XANES LCFs (Table S3). This suggests effective sorption of As(V) generated via As(III) oxidation by ROS, formed during Fe(II) reactions with both $O_2$ or $H_2O_2$, since direct oxidation of As(III) by $O_2$ or $H_2O_2$ in the experimental time frame (30 min) was not feasible (Hug and Leupin, 2003).

Combining the aqueous As(III) removal results with the measurements of As oxidation state on the solids (with XANES LCFs) and in solution (with anionic exchange resins) yields the speciation plot given in Fig. 2(C). This plot reveals that, while overall aqueous As(III) removal increased with increasing initial $H_2O_2$ concentration, the majority of As bound to the solids was always As(V) and the majority of residual aqueous As was As(III) for all oxidant conditions. For example, in the $O_2$ system As(V) accounted for 2.2 μM of the total adsorbed As content of 3.0 μM (72%), whereas 80% of the 3.8 μM residual As was As(III). Similarly, in the $H_2O_2$ system, As(V) was 100% of the adsorbed As and As(III) accounted for 72% of the 0.4 μM residual As. These trends were reproduced in the sequential $H_2O_2$+$O_2$ system (Fig. 2(C)) and are consistent with the orders of magnitude higher sorption affinity of As(V) than As(III) (Roberts et al., 2004). Although the fraction of As(V) and As (III) bound to the solids was similar among many of the samples, the total amount of oxidized As(III) increased with increasing $H_2O_2$ concentration (i.e. total As(V) increased from 2.9 μM in the $O_2$ system to >6 μM in the $H_2O_2$ system). The increase in As(III) oxidation with $H_2O_2$ concentration is consistent with more effective ROS generation when Fe (II) is oxidized by $H_2O_2$ compared to $O_2$ (Hug and Leupin, 2003), which is attributed to the 1:1 stoichiometric yield of ROS when Fe(II) reacts

with $H_2O_2$ compared to the 1:3 yield of ROS when Fe(II) reacts with $O_2$.

Combining the As speciation plots in Fig. 2(C) and the solid-phase Fe speciation plots in Fig. 1(C) uncovers a key finding about the anaerobic co-oxidation of As(III) and Fe(II) by $H_2O_2$. Comparing the overall As removal between the $O_2$ experiment and the sequential 40 μM $H_2O_2$+$O_2$ experiment showed a decrease in the residual As concentration from 3.8 μM to 1.3 μM, a difference of 2.5 μM As when 40 μM $H_2O_2$ was applied, whereas for the same samples, the total amount of oxidized As(III) was 2.9 μM for the $O_2$ experiment and 4.8 μM for the sequential 40 μM $H_2O_2$+$O_2$ experiment, a difference of only 1.9 μM As. The higher overall As removal efficacy for the 40 μM $H_2O_2$+$O_2$ experiment, cannot be attributed to an increase in As(III) oxidation alone. Therefore, the results indicate that the higher reactive surface area of the poorly-ordered solids generated by Fe(II) oxidation with $H_2O_2$ played a critical role in improving overall As removal efficacy.

### 3.3. Under- and over-dosage of $H_2O_2$

Experiments were performed to identify any benefit from dosing $H_2O_2$ below or above the stoichiometric amount required to anaerobically oxidize 100±3 μM Fe(II). Fig. 3(A) shows the concentration of oxidized Fe(II) and the corresponding removal of the initial 7±0.2 μM As (III) as a function of different $H_2O_2$ dosages (10-400 μM) at t = 30 min. As the $H_2O_2$ concentration increased, the concentration of oxidized Fe (II) also increased up to the complete oxidation of Fe(II) at $H_2O_2$ concentrations above 60 μM. For $H_2O_2$ dosages below 60 μM (i.e., under-dosage; 10-40 μM), only partial oxidation of 100±3 μM Fe(II) was observed (20-80% oxidation). However, the ratio of generated Fe(III) to dosed $H_2O_2$ remained around 2:1 mol:mol for all conditions (Fig. 3(A)), indicating that the 2:1 stoichiometry of Fe(II) oxidation by $H_2O_2$ was maintained.

The results from the sequential $H_2O_2$+$O_2$ experiments were consistent with the findings mentioned above. Increasing the $H_2O_2$ concentration from 10-40 μM, which is below the required amount for 100% Fe (II) oxidation, resulted in improved As removal due to the formation of more Fe(III) precipitates (Section 3.1 and 3.2). For instance, with 10 μM $H_2O_2$ the residual As concentration (t = 30 min) was 4.8±0.2 μM (31% removal), which decreased to 1.7±0.1 μM (76% removal) with 40 μM $H_2O_2$ (Fig. 3(A)). However, we also observed that increasing the $H_2O_2$ concentration above the amount required to completely oxidize 100±3 μM Fe(II) (i.e., over-dosage) also improved As(III) removal. For example, when the $H_2O_2$ dosage increased from 60 to 400 μM (i.e., over-dosage), the dissolved As concentration at t = 30 min decreased from 0.6±0.1 (92% removal) to 0.1±0.1 μM (98.5% removal), which resulted in As levels below the WHO recommended limit (<0.13 μM) (Fig. 3(A)). This increase in As removal can be explained by the oxidation of As(III) to As (V) via ROS, formed by decomposition of $H_2O_2$ on the surface of Fe(III) precipitates (Lin and Gurol, 1998), with subsequent sorption of As(V).

Finally, we noted that the removal of the initial 7±0.2 μM As(III) with 400 μM $H_2O_2$ (98.5% removal) was almost equal to the removal of the initial 7±0.5 μM As(V) (99.3% removal; at 60 μM $H_2O_2$), when a similar Fe dosage of 100±3 μM was used (Fig. 3(B)). This result highlights the advantage of using $H_2O_2$, because previous Fe(II)-based As removal studies, with only $O_2$ dosing, have always reported higher removals of initial As(V) compared to As(III) (Kumar et al., 2004; Roberts et al., 2004; Roy et al., 2020; Wan et al., 2011).

### 3.4. Application to raw anaerobic groundwater

To validate that enhanced As(III) co-removal can be achieved by adding $H_2O_2$ to groundwater containing native Fe(II), experiments were performed with raw anaerobic groundwater rich in Fe(II), co-occurring As(III), and other native dissolved species (such as phosphorous (total P) and manganese (Mn)). Fig. 4 shows the removal of initial As(III), Mn, and total P from raw anaerobic groundwater with Fe(III) generation over 30 min. Consistent with the laboratory experiments (Sections 3.1 and 3.2), all groundwater-native Fe(II) was oxidized with $H_2O_2$ and rapidly formed precipitates (within 2 min), whereas $O_2$ oxidation of Fe (II) required the full 30 min of the experiment. During the $H_2O_2$ dosing experiment, As(III) was also quickly removed, with 97.6% As(III) removal measured in 2 min. When the native Fe(II) in groundwater was oxidized by $O_2$, As(III) removal continued over the full 30 min reaction duration and at the end of the experiment 1.3±0.1 μM residual As (81% removal) remained in solution.

While our experiments with natural groundwater were consistent with the laboratory experiments (i.e., $H_2O_2$ addition outperformed

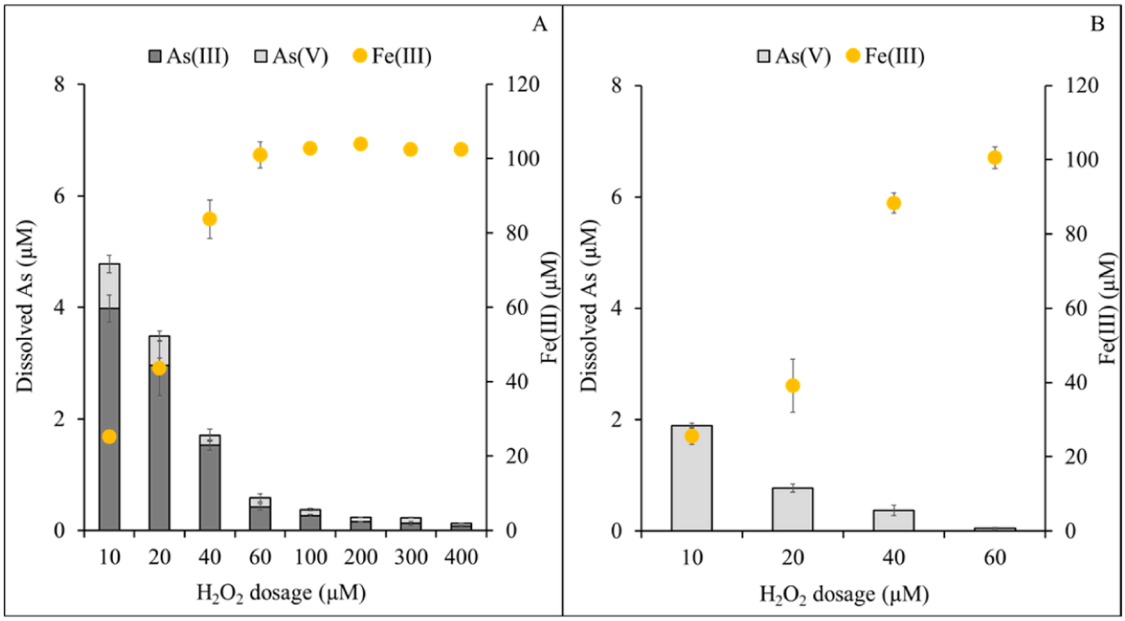


**Fig. 3.** Dissolved As and Fe(III) concentration in solutions at t = 30 min plotted as a function of different $H_2O_2$ dosage when 100±3 μM of Fe(II) was oxidized by 10-400 μM $H_2O_2$ anaerobically. Solutions initially contained 7±0.2 μM As(III) (A) or 7±0.5 μM As(V) (B), 2.5 mM $NaHCO_3$, and 10 mM NaCl. All Fe(III) formed solids and no dissolved Fe(III) was measured (data not shown). Data points and error bars represent the average and standard deviation of the samples obtained from replicate experiments.

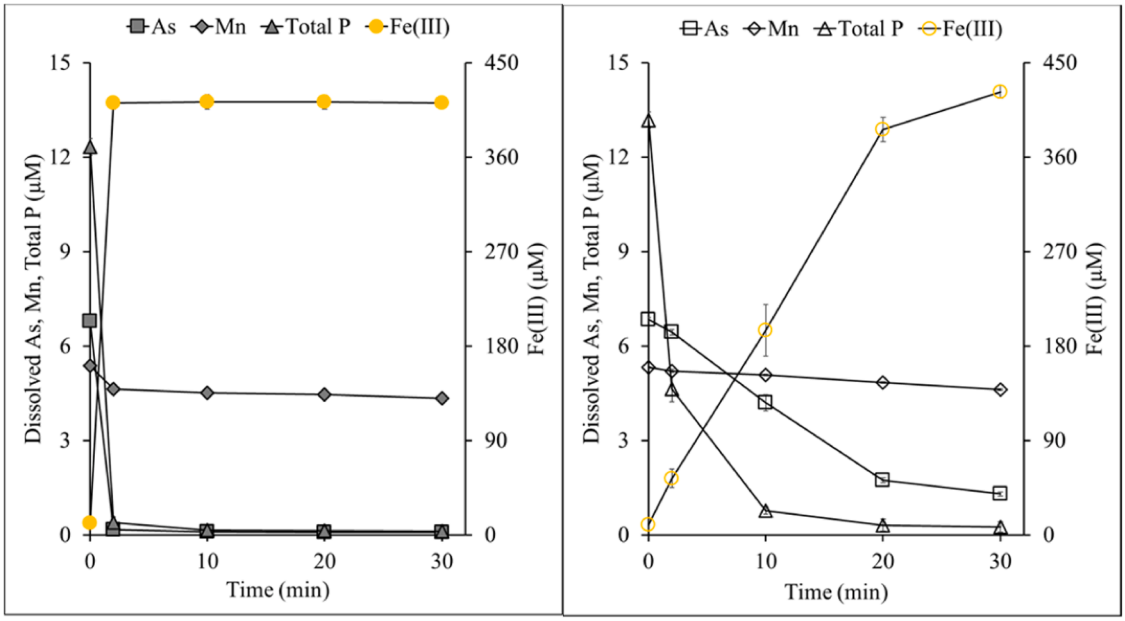


**Fig. 4.** As, Mn, and total P removal from raw anaerobic groundwater as function of time and Fe(III) generation when 424±12 μM groundwater-native Fe(II) was completely oxidized by 800 μM $H_2O_2$ (left) and 8.0-9.0 mg/L $O_2$ (right). Solutions initially contained 6.8±0.1 μM As(III); 5.3±0.1 μM Mn, and 12.7±0.5 μM total P. All Fe(III) formed solids and no dissolved Fe(III) was measured (data not shown). Data points and error bars represent the average and standard deviation of the samples obtained from replicate experiments.

aeration), some key differences were observed. First, compared to the laboratory experiments, raw groundwater samples showed a better removal of As(III) for both $H_2O_2$ and $O_2$ oxidation. Second, the difference between As(III) removal using $H_2O_2$ or $O_2$ was smaller for the raw groundwater experiments. The less distinct As removal of $H_2O_2$ and $O_2$ oxidants applied to natural groundwater could be attributed to the four times higher Fe(II) concentration in natural groundwater than in the laboratory experiments, which suggests that optimal conditions for enhancing As removal by $H_2O_2$ addition occur at lower initial Fe(II) levels.

Additionally, the optimal removal of As(III) with $H_2O_2$ in groundwater containing low levels of native Fe(II) can also be impacted by the presence of other native species that can compete for adsorption sites and ROS. For example, phosphorous in groundwater is present mainly as phosphate ($PO_4^{3-}$) and studies have shown its competition with As(V) for adsorption sites on Fe solids (Roberts et al., 2004). As observed in Fig. 4, along with the removal of As(III), total P removal was also observed for both $H_2O_2$ and $O_2$ experiments, but the removal of total P was different for the different oxidants. In the $O_2$ experiment, the rate and amount of total P removal was higher than As(III), whereas the $H_2O_2$ experiment did not display a substantial difference between As(III) and total P removal. This result can be explained by the availability of sufficient sorption sites for both As and P on the Fe solids owing to the formation of poorly-ordered solids during $H_2O_2$ oxidation, the high Fe(II) concentration (424±12 μM), and to the enhanced oxidation of As(III) using $H_2O_2$. However, in situations where native Fe(II) is low, a possible lower co-removal of As(III) could be expected due to competition with $PO_4^{3-}$ for adsorption sites.

Apart from $PO_4^{3-}$, groundwater can also contain dissolved Mn, which might impact As(III) co-removal with native Fe(II). For instance, previous studies have reported that Mn in groundwater, which is present as Mn(II), can compete with As(III) for ROS, yielding oxidized Mn(III) that (partially) incorporates into the co-precipitating Fe(III) solids (Ahmad et al., 2019; Catrouillet et al., 2020; van Genuchten and Peña, 2017). However as shown in Fig. 4, Mn removal was relatively low for both $H_2O_2$ (19% removal) and $O_2$ (13% removal), suggesting that Mn(III) formation was not substantial. However, since identifying the solid-phase speciation of Mn was beyond the scope of this study, it is not clear whether there was any competition between Mn(II) and As(III) for the generated ROS.

### 3.5. Implications for groundwater treatment

We observed improved As(III) removal when co-existing Fe(II) was oxidized by $H_2O_2$ rather than $O_2$. The ratio of As(III) removed to Fe(III) generated increased from 0.03 to 0.06 mol:mol when 100 μM Fe(II) was completely oxidized with either 8.0-9.0 mg/L $O_2$ or 100 μM $H_2O_2$, respectively, indicating substantially less Fe is required for equivalent As removal with $H_2O_2$. The application of such Fenton-type systems (i.e., Fe(II)+$H_2O_2$) to improve As(III) removal from water has been reported previously. For example, Krishna et al. (2001) showed that initial treatment of 2 mg/L As(III) with 100 mg/L Fe(II) and 100 μL/L of 30% $H_2O_2$, followed by passing through zero valent iron columns and a sand bed, achieved As removal to <10 μg/L (WHO guideline). In addition, Wang et al. (2013) observed that oxidizing 20 μM Fe(II) with 50 μM $H_2O_2$ at pH 7.0 resulted in 70% oxidation of 20 μM As(III) compared to just 2.5% while oxidizing the Fe(II) with $O_2$. While these studies are useful, they interpret their results primarily by improved As(III) co-oxidation by ROS and did not focus on the influence of Fe(III) precipitate structure. In this study, we also observed that the improved As(III) co-removal by $H_2O_2$ is partly attributed to the well-established enhanced efficiency of As(III) oxidation in Fe(II)+$H_2O_2$ systems due to higher stoichiometric yield of ROS compared to Fe(II)+$O_2$ systems (Bandaru et al., 2020; Hug and Leupin, 2003). However, our results explicitly showed that the Fe(III) precipitate structure played a major role in improving As(III) removal. The Fe K-edge EXAFS analysis performed in this study indicated a systematic decrease in precipitate crystallinity (i.e., increase in reactive specific surface area) from moderately crystalline Lp in the $O_2$ system to poorly-ordered Fe(III) precipitates with $H_2O_2$ (Fig. 1(C)). This impact of Fe(III) precipitate structure is often overlooked in Fe-based As removal techniques, but we show that the type of Fe(III) precipitates must be considered to accurately predict As removal in groundwater treatment.

Our results also indicated that oxidizing the groundwater-native Fe(II) anaerobically with $H_2O_2$ prior to aeration-filtration can be used to leverage the full potential of native Fe(II) for As(III) treatment.

Depending on the initial As:Fe and Fe:$H_2O_2$ ratios, this novel approach can remove As(III) to below drinking water standards, achieving a high As(III) removal, which is often difficult with conventional aeration-filtration. The optimal use of native Fe(II) via $H_2O_2$ oxidation can help to avoid the need for additional Fe dosage (as $FeCl_3$) in situations where oxidizing native Fe(II) by aeration is not sufficient to meet As drinking water limits. This reduction of Fe dosage will also lower the volume of generated Fe sludge and thus lower the frequency of filter backwashing. Additionally, anaerobic oxidation of Fe(II) with $H_2O_2$ prior to aeration will not result in the same increase in groundwater pH as is observed during aeration due to degassing of $CO_{2(g)}$. As long as Fe(II) is oxidized, maintaining a low pH is advantageous because As(V) adsorption to Fe solids decreases with increasing pH (Annaduzzaman et al., 2021b; Dixit and Hering, 2003).

Usage of other strong oxidants (such as $KMnO_4$ or NaOCl) during aeration-filtration has been reported previously, effectively oxidizing As (III) and also generating poorly-ordered Fe solids (van Genuchten and Ahmad, 2020). However, compared to those oxidants, $H_2O_2$ is considered a green oxidant, because its by-products, namely $H_2O$ and $O_2$, are benign (Goyal et al., 2020; Pham et al., 2012b; Zhao et al., 2019). Recent studies have also shown that $H_2O_2$ can be electrochemically generated *in-situ* (Bandaru et al., 2020), which eliminates the necessity to maintain chemical stocks of $H_2O_2$ on site, thus decreasing the supply chain for operating groundwater treatment plants.

The results in this work suggest that oxidizing groundwater-native Fe (II) with $H_2O_2$ anaerobically prior to aeration-filtration can be a novel approach to optimize the co-removal of toxic As(III). However, our study did not take into account potentially different environmental scenarios that can impact As(III) removal. For example, the laboratory experiments were performed in controlled conditions with a fixed Fe(II):As(III) ratio and pH, and without the presence of other competing ions. While a set of experiments with raw anaerobic groundwater was performed, the advantage of oxidizing native Fe(II) with $H_2O_2$ over $O_2$ for As(III) co-removal diminished most likely due to the high concentration of native Fe(II). In the experiments with real groundwater, although 1 mol of $H_2O_2$ is sufficient to oxidize 2 mol of Fe(II), an excess $H_2O_2$ was dosed to minimize the impact of any atmospheric $O_2$ influx and to ensure complete oxidation of the native Fe(II) by $H_2O_2$ in absence of $N_{2(g)}$ dosage as in laboratory experiments. While our laboratory investigations and tests in real groundwater highlight the potential benefits of $H_2O_2$ dosing, it is recommended to perform further studies with real anaerobic groundwater under various environmental conditions, with optimization of the $H_2O_2$ dosage, to further validate the novelty of the proposed approach. Overall, the advantage of anaerobic $H_2O_2$ oxidation of native Fe(II) for As(III) removal is that it can be easily implemented in conventional or decentralized systems to treat As contaminated groundwater without major changes in infrastructure and without substantial increases in treatment costs.

## Conclusions

In this study, we showed a novel approach where the co-removal of groundwater As(III) with native Fe(II) can be enhanced by oxidizing the Fe(II) anaerobically with $H_2O_2$ prior to aeration-filtration rather than conventionally by aeration (or $O_2$) under aerobic conditions. The enhanced As(III) co-removal with $H_2O_2$ was partly due to generation of a larger fraction of poorly-ordered Fe(III) solids with a higher reactive specific surface area compared to moderately crystalline Fe(III) solids generated by $O_2$ as well as the generation of more ROS per mole of Fe(II) when dosing $H_2O_2$ (1:1) compared to $O_2$ (1:3), thus favouring As(III) oxidation to readily adsorbed As(V). Hence, we propose the application of $H_2O_2$, a green oxidant, for anaerobic Fe(II) and As(III) co-oxidation in groundwater treatment prior to aeration to optimize native Fe(II) usage, which will reduce the volume of generated sludge.

## CrediT authorship contribution statement

**Mrinal Roy**: Analysis Data**, Case M. van Genuchten:** Analysis Data, XAS analysis; guidance on design; for XAS, **Luuk Rietveld:** and guidance on design, **Doris van Halem:** guidance on design, Analysis Data

## CRediT authorship contribution statement

**Mrinal Roy:** Conceptualization, Data curation, Investigation, Methodology, Visualization, Validation, Software, Writing – original draft. **Case M. van Genuchten:** Supervision, Conceptualization, Software, Visualization, Writing – review & editing. **Luuk Rietveld:** Supervision, Conceptualization, Writing – review & editing. **Doris van Halem:** Supervision, Conceptualization, Visualization, Writing – review & editing.

## Declaration of Competing Interest

The authors declare that they have no known competing financial interests or personal relationships that could have appeared to influence the work reported in this paper.

## Data availability

Data will be made available on request.

## Acknowledgments

This project is supported by TKI Watertechnology, Top Sector Water. The authors want to thank Jane Erkemeij and Patricia van den Bos for their help in ICP-MS analysis and Erik Kraaijeveld for his help while performing the experiments in the lab and in the treatment plant. Use of SSRL, SLAC National Accelerator Laboratory, was supported by the U.S. Department of Energy, Office of Science, Basic Energy Sciences, under Contract No. DE-AC02-76SF00515.

## Supplementary materials

Supplementary material associated with this article can be found, in the online version, at doi:10.1016/j.watres.2022.119007.

## References

Ahmad, A., van der Wal, A., Bhattacharya, P., van Genuchten, C.M., 2019. Characteristics of Fe and Mn bearing precipitates generated by Fe(II) and Mn(II) co-oxidation with $O_2$, $MnO_4$ and HOCl in the presence of groundwater ions. Water Res. 161 (June), 505–516. https://doi.org/10.1016/j.watres.2019.06.036.

Annaduzzaman, M., Bhattacharya, P., Biswas, A., Hossain, M., Ahmed, K.M., van Halem, D., 2018. Arsenic and manganese in shallow tubewells: validation of platform color as a screening tool in Bangladesh. Groundwater Sustain. Dev. 6, 181–188. https://doi.org/10.1016/J.GSD.2017.11.008.

Annaduzzaman, M., Rietveld, L.C., Ghosh, D., Hoque, B.A., van Halem, D., 2021a. Anoxic storage to promote arsenic removal with groundwater-native iron. Water Res. 202 https://doi.org/10.1016/J.WATRES.2021.117404.

Annaduzzaman, M., Rietveld, L.C., Hoque, B.A., Bari, M.N., van Halem, D., 2021b. Arsenic removal from iron-containing groundwater by delayed aeration in dual-media sand filters. J. Hazard. Mater. 411, 124823 https://doi.org/10.1016/J.JHAZMAT.2020.124823.

Bandaru, S.R.S., Van Genuchten, C.M., Kumar, A., Glade, S., Hernandez, D., Nahata, M., Gadgil, A., 2020. Rapid and efficient arsenic removal by iron electrocoagulation enabled with *in situ* generation of hydrogen peroxide. Environ. Sci. Technol. 54 (10), 6094–6103. https://doi.org/10.1021/acs.est.0c00012.

Bissen, M., Frimmel, F.H., 2003. Arsenic — a review. Part II: oxidation of arsenic and its removal in water treatment. Acta Hydroch. Hydrob. 31 (2), 97–107. https://doi.org/10.1002/AHEH.200300485.

Bora, A.J., Gogoi, S., Baruah, G., Dutta, R.K., 2016. Utilization of co-existing iron in arsenic removal from groundwater by oxidation-coagulation at optimized pH. J. Environ. Chem. Eng. 4 (3), 2683–2691. https://doi.org/10.1016/J.JECE.2016.05.012.

Catrouillet, C., Hirosue, S., Manetti, N., Boureau, V., Peña, J., 2020. Coupled As and Mn redox transformations in an Fe(0) electrocoagulation system: competition for

reactive oxidants and sorption sites. Environ. Sci. Technol. 54 (12), 7165–7174. https://doi.org/10.1021/acs.est.9b07099.
Dixit, S., Hering, J.G., 2003. Comparison of arsenic(V) and arsenic(III) sorption onto iron oxide minerals: implications for arsenic mobility. Environ. Sci. Technol. 37 (18), 4182–4189. https://doi.org/10.1021/ES030309T.
Goyal, R., Singh, O., Agrawal, A., Samanta, C., Sarkar, B., 2020. Advantages and limitations of catalytic oxidation with hydrogen peroxide: from bulk chemicals to lab scale process. Catal. Rev. Sci. Eng. 64 (2), 229–285. https://doi.org/10.1080/01614940.2020.1796190/FORMAT/EPUB.
Gude, J.C.J., Rietveld, L.C., van Halem, D., 2016. Fate of low arsenic concentrations during full-scale aeration and rapid filtration. Water Res. 88, 566–574. https://doi.org/10.1016/j.watres.2015.10.034.
Gude, J.C.J., Rietveld, L.C., van Halem, D., 2017. As(III) oxidation by $MnO_2$ during groundwater treatment. Water Res. 111, 41–51. https://doi.org/10.1016/j.watres.2016.12.041.
Gude, J.C.J., Rietveld, L.C., van Halem, D., 2018. Biological As(III) oxidation in rapid sand filters. J. Water Process Eng. 21, 107–115. https://doi.org/10.1016/j.jwpe.2017.12.003.
Holm, T.R., Wilson, S.D., 2006. Chemical oxidation for arsenic removal. MTAC Publ. TR06. *-05*.
Hug, S.J., Leupin, O., 2003. Iron-catalyzed oxidation of Arsenic(III) by oxygen and by hydrogen peroxide: pH-dependent formation of oxidants in the Fenton reaction. Environ. Sci. Technol. 37 (12), 2734–2742. https://doi.org/10.1021/es026208x.
Kapaj, S., Peterson, H., Liber, K., Bhattacharya, P., 2006. Human health effects from chronic arsenic poisoning - a review. J. Environ. Sci. Health - Part A Toxic/Hazard. Substances Environ. Eng. 41 (10), 2399–2428. https://doi.org/10.1080/10934520600873571.
King, D.W., 1998. Role of carbonate speciation on the oxidation rate of Fe(II) in aquatic systems. Environ. Sci. Technol. 32 (19), 2997–3003. https://doi.org/10.1021/ES980206O/SUPPL_FILE/ES980206O_S.PDF.
King, D.W., Farlow, R., 2000. Role of carbonate speciation on the oxidation of Fe(II) by $H_2O_2$. Mar. Chem. 70 (1–3), 201–209. https://doi.org/10.1016/S0304-4203(00)00026-8.
Krishna, M.V.B., Chandrasekaran, K., Karunasagar, D., Arunachalam, J., 2001. A combined treatment approach using Fenton's reagent and zero valent iron for the removal of arsenic from drinking water. J. Hazard. Mater. 84 (2–3), 229–240. https://doi.org/10.1016/S0304-3894(01)00205-9.
Kumar, P.R., Chaudhari, S., Khilar, K.C., Mahajan, S.P., 2004. Removal of arsenic from water by electrocoagulation. Chemosphere 55 (9), 1245–1252. https://doi.org/10.1016/j.chemosphere.2003.12.025.
Li, Y., Bland, G.D., Yan, W., 2016. Enhanced arsenite removal through surface-catalyzed oxidative coagulation treatment. Chemosphere 150, 650–658. https://doi.org/10.1016/j.chemosphere.2016.02.006.
Lin, S.S., Gurol, M.D., 1998. Catalytic decomposition of hydrogen peroxide on iron oxide: kinetics, mechanism, and implications. Environ. Sci. Technol. 32 (10), 1417–1423. https://doi.org/10.1021/es970648k.
Pedersen, H.D., Postma, D., Jakobsen, R., Larsen, O., 2005. Fast transformation of iron oxyhydroxides by the catalytic action of aqueous Fe(II). Geochim. Cosmochim. Acta 69 (16), 3967–3977. https://doi.org/10.1016/J.GCA.2005.03.016.
Pham, A.L.T., Doyle, F.M., Sedlak, D.L., 2012a. Inhibitory effect of dissolved silica on $H_2O_2$ decomposition by iron(III) and manganese(IV) oxides: implications for $H_2O_2$-based *in situ* chemical oxidation. Environ. Sci. Technol. 46 (2), 1055–1062. https://doi.org/10.1021/es203612d.
Pham, A.L.T., Doyle, F.M., Sedlak, D.L., 2012b. Kinetics and efficiency of $H_2O_2$ activation by iron-containing minerals and aquifer materials. Water Res. 46 (19), 6454–6462. https://doi.org/10.1016/J.WATRES.2012.09.020.
Podgorski, J., Berg, M., 2020. Global threat of arsenic in groundwater. Science 368 (6493), 845–850. https://doi.org/10.1126/science.aba1510.
Roberts, L.C., Hug, S.J., Ruettimann, T., Billah, M., Khan, A.W., Rahman, M.T., 2004. Arsenic removal with iron(II) and iron(III) in waters with high silicate and phosphate concentrations. Environ. Sci. Technol. 38 (1), 307–315. https://doi.org/10.1021/es0343205.
Roy, M., van Genuchten, C.M., Rietveld, L., van Halem, D., 2020. Integrating biological As(III) oxidation with Fe(0) electrocoagulation for arsenic removal from groundwater. Water Res. 188, 116531 https://doi.org/10.1016/j.watres.2020.116531.
Sharma, A.K., Sorlini, S., Crotti, B.M., Collivignarelli, M.C., Tjell, J.C., Abbà, A., 2016. Enhancing arsenic removal from groundwater at household level with naturally occurring iron. Rev. Ambiente Água 11 (3), 486–498. https://doi.org/10.4136/AMBI-AGUA.1815.
Toner, B.M., Santelli, C.M., Marcus, M.A., Wirth, R., Chan, C.S., McCollom, T., Bach, W., Edwards, K.J., 2009. Biogenic iron oxyhydroxide formation at mid-ocean ridge hydrothermal vents: Juan de Fuca Ridge. Geochim. Cosmochim. Acta 73 (2), 388–403. https://doi.org/10.1016/j.gca.2008.09.035.
Tseng, W.P., 1977. Effects and dose response relationships of skin cancer and blackfoot disease with arsenic. Environ. Health Perspect. Vol.19, 109–119. https://doi.org/10.1289/ehp.7719109.
van Genuchten, C.M., Behrends, T., Kraal, P., Stipp, S.L.S., Dideriksen, K., 2018. Controls on the formation of Fe(II,III) (hydr)oxides by Fe(0) electrolysis. Electrochim. Acta 286, 324–338. https://doi.org/10.1016/j.electacta.2018.08.031.
van Genuchten, C M, Pena, J., 2017. Mn(II) oxidation in fenton and fenton type systems: identification of reaction efficiency and reaction products. Environ. Sci. Technol. 51 (5), 2982–2991. https://doi.org/10.1021/acs.est.6b05584.
van, Genuchten, Case, M., Addy, S.E.A., Peña, J., Gadgil, A.J., 2012. Removing arsenic from synthetic groundwater with iron electrocoagulation: an Fe and As K-edge EXAFS study. Environ. Sci. Technol. 46 (2), 986–994. https://doi.org/10.1021/es201913a.
van, Genuchten, Case, M., Ahmad, A., 2020. Groundwater as removal by As(III), Fe(II), and Mn(II) Co-oxidation: contrasting as removal pathways with $O_2$, NaOCl, and $KMnO_4$. Environ. Sci. Technol. 54 (23), 15454–15464. https://doi.org/10.1021/acs.est.0c05424.
van, Genuchten, Case, M, Gadgil, A.J., Peña, J., 2014. Fe(III) nucleation in the presence of bivalent cations and oxyanions leads to subnanoscale 7 Å polymers. Environ. Sci. Technol 48 (21). https://doi.org/10.1021/es503281a.
Wan, W., Pepping, T.J., Banerji, T., Chaudhari, S., Giammar, D.E., 2011. Effects of water chemistry on arsenic removal from drinking water by electrocoagulation. Water Res. 45 (1), 384–392. https://doi.org/10.1016/j.watres.2010.08.016.
Wang, Z., Bush, R.T., Liu, J., 2013. Arsenic(III) and iron(II) co-oxidation by oxygen and hydrogen peroxide: divergent reactions in the presence of organic ligands. Chemosphere 93 (9), 1936–1941. https://doi.org/10.1016/j.chemosphere.2013.06.076.
Webb, S.M., 2005. SIXpack: a graphical user interface for XAS analysis using IFEFFIT. Phys. Scr. T T115 (T115), 1011–1014. https://doi.org/10.1238/Physica.Topical.115a01011.
Zhao, H., Li, Z., Jin, J., 2019. Green oxidant $H_2O_2$ as a hydrogen atom transfer reagent for visible light-mediated Minisci reaction. New J. Chem. 43 (32), 12533–12537. https://doi.org/10.1039/C9NJ03106E.